JACS
JOURNAL OF THE AMERICAN CHEMICAL SOCIETY

Article

pubs.acs.org/JACS

H_2O_2-Activatable and O_2-Evolving Nanoparticles for Highly Efficient and Selective Photodynamic Therapy against Hypoxic Tumor Cells

Huachao Chen,† Jiangwei Tian,† Weijiang He,* and Zijian Guo*

State Key Laboratory of Coordination Chemistry, Coordination Chemistry Institute, School of Chemistry and Chemical Engineering, Nanjing University, Nanjing 210093, P.R. China

Supporting Information

ABSTRACT: The low selectivity of currently available photosensitizers, which causes the treatment-related toxicity and side effects on adjacent normal tissues, is a major limitation for clinical photodynamic therapy (PDT) against cancer. Moreover, since PDT process is strongly oxygen dependent, its therapeutic effect is seriously hindered in hypoxic tumor cells. To overcome these problems, a cell-specific, H_2O_2-activatable, and O_2-evolving PDT nanoparticle (HAOP NP) is developed for highly selective and efficient cancer treatment. The nanoparticle is composed of photosensitizer and catalase in the aqueous core, black hole quencher in the polymeric shell, and functionalized with a tumor targeting ligand c(RGDfK). Once HAOP NP is selectively taken up by $\alpha_v\beta_3$ integrin-rich tumor cells, the intracellular H_2O_2 penetrates the shell into the core and is catalyzed by catalase to generate O_2, leading to the shell rupture and release of photosensitizer. Under irradiation, the released photosensitizer induces the formation of cytotoxic singlet oxygen ($^1O_2$) in the presence of O_2 to kill cancer cells. The cell-specific and H_2O_2-activatable generation of $^1O_2$ selectively destroys cancer cells and prevents the damage to normal cells. More significantly, HAOP NP continuously generates O_2 in PDT process, which greatly improves the PDT efficacy in hypoxic tumor. Therefore, this work presents a new paradigm for H_2O_2-triggered PDT against cancer cells and provides a new avenue for overcoming hypoxia to achieve effective treatment of solid tumors.

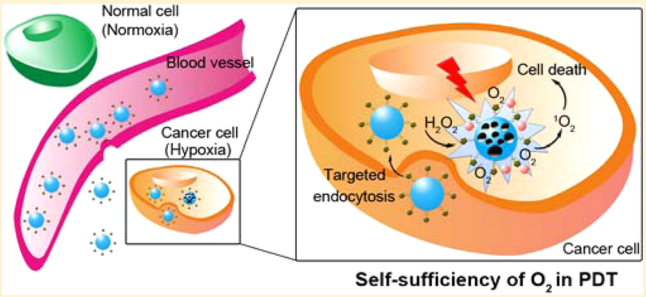

INTRODUCTION

Photodynamic therapy (PDT) is a clinical modality that employs a photosensitizer, an appropriate excitation light, and oxygen (O_2) molecules to generate cytotoxic singlet oxygen ($^1O_2$) for the treatment of many localized and superficial cancers.[1] PDT has several advantages over conventional therapies because of its noninvasive nature, the fast healing process resulting in little or no scarring, and the ability to treat patients in an outpatient setting.[2] Over the past decade, various strategies have been explored for enhancing the $^1O_2$ generation efficiency of photosensitizers and controlling their photodynamic action to improve the PDT efficacy and selectivity.[3] Although PDT has become a promising treatment option for early stage cancer and an adjuvant for surgery in late-stage cancer, tumor hypoxia severely reduced the therapeutic efficiency and constitutes an obstacle to the clinical application of PDT.[4] Hypoxia, which is caused by an inadequate oxygen supply, is increasingly being recognized as a characteristic feature of solid tumors.[5] This hypoxic environment within a tumor is highly detrimental to photosensitizers that require molecular oxygen to mediate their cytotoxic effects.[6] Furthermore, the photosensitizer-mediated consumption of O_2 during PDT further potentiates tumor hypoxia.[7] Thus, the application of traditional PDT agents is significantly limited by the tumor hypoxia due to the O_2-dependent nature of PDT.[8] To address this problem, efforts have been made to develop new O_2-independent phototherapy agents, for instance, inducing pH imbalance within the cytosol by a photoacid generator.[9] As an alternative approach, smart system which combines O_2 evolving and PDT process would prove more convenient for overcoming tumor hypoxia in the application of traditional PDT agents.

Another obstacle of PDT is the limited tumor selectivity which causes damage to adjacent healthy tissues.[10] To improve the tumor selectivity, "activatable PDT" agents that can be activated by tumor-associated stimuli have received considerable attention to minimize nonspecific activation of phototoxicity.[11] In the inactive state, the photosensitizer remains in a quenched conformation and generates only a small amount of $^1O_2$ under irradiation. Upon interactions with acids,[12a] thiols,[12b] cancer-related proteases,[12c] and nucleic acids,[12d] their optical properties could be selectively activated. Thus, "activatable PDT" can specifically kill diseased cells that differ from normal cells by exploiting the unique pathological environment in tumor. Recent reports have indicated that most cancer cells exhibit increased oxidative stress,[13] features that could be valuable in the development of reactive oxygen species (ROS)

Received: November 6, 2014
Published: January 9, 2015

DOI: 10.1021/ja511420n
J. Am. Chem. Soc. 2015, 137, 1539−1547

activatable PDT strategies. To date, several H_2O_2-responsive nanocarriers have been developed for controllable drug release.[14] However, H_2O_2-activatable photosensitizers that can response to biologically relevant oxidative conditions remain very rare.

We herein developed a H_2O_2-activatable and O_2-evolving PDT nanoparticle (HAOP NP) for controllable $^1O_2$ release, achieving self-sufficiency of O_2 in the PDT process (Scheme 1).

Scheme 1. Schematic Illustration of (a) Mechanism of H_2O_2-Controllable Release of Photosensitizer and O_2 to Implement PDT[a] and (b) HAOP NP for Selective and Efficient PDT against Hypoxic Tumor Cell

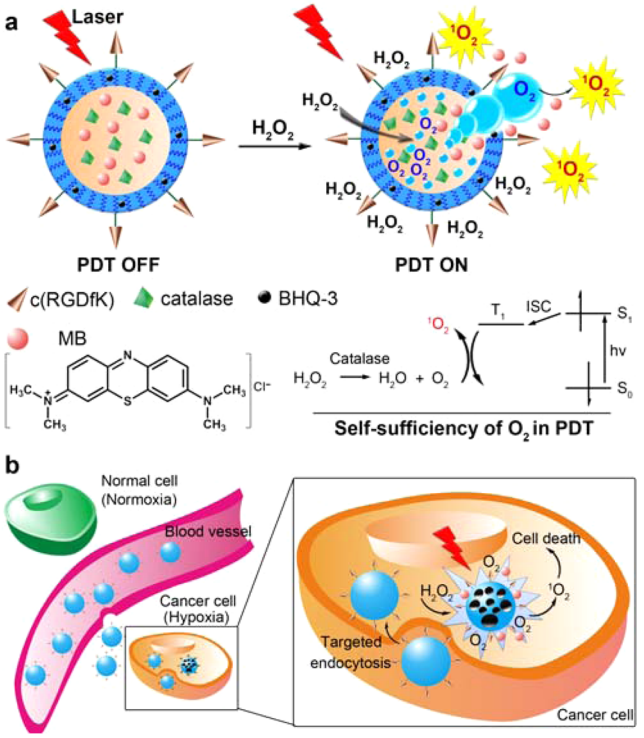

[a] S_0, singlet ground state; S_1, lowest singlet excited state; T_1, lowest triplet excited state; ISC, intersystem crossing.

In this study, poly(D,L-lactic-*co*-glycolic acid) (PLGA) was chosen as the drug carrier for its biocompatibility and biodegradability.[15] Methylene blue (MB) was used as a typical example of photosensitizer due to its high quantum yield of $^1O_2$ generation ($\Phi_\Delta \sim 0.5$) in the excitation of the therapeutic window (600−900 nm).[16] Catalase, which was previously reported by our group that can be an O_2-evolving agent for drug release,[14a] was incorporated into the aqueous core of NPs together with MB. Black hole quencher-3 (BHQ-3) was doped into the PLGA shell, serving as an ultraefficient energy quencher of excited photosensitizer. When incorporated into the NP, the $^1O_2$ production of MB was "switched off" due to the efficient quenching of excited-state energy by BHQ-3 owing to the Förster resonance energy transfer (FRET) mechanism. Once H_2O_2 penetrated into the core of NP, it was catalyzed by catalase to quickly generate O_2 gas, causing the rupture of PLGA shell and subsequent release of MB. As a result, FRET efficiency was decreased, and the $^1O_2$ production was "switched on" (Scheme 1a). To further improve the cancer selectivity, a cyclic pentapeptide c(RGDfK) as the targeting ligand was conjugated on the surface of NP. After injected into the blood vessel, the HAOP NP could be accumulated into the tumor tissue and selectively taken up by $\alpha_v\beta_3$ integrin-rich cancer cells, in which the high level of intracellular H_2O_2 activated the NP to produce $^1O_2$ for killing cancer cells (Scheme 1b). The integrating utilization of c(RGDfK) and H_2O_2 led to a significant enhancement of PDT selectivity to cancer. Moreover, the O_2 generated in PDT process efficiently improved the therapeutic effect through overcoming the hypoxic problems in tumor tissue. To the best of our knowledge, it is reported for the first time that a PDT agent can achieve not only H_2O_2-controllable release of $^1O_2$ but also self-sufficiency of O_2 in hypoxic tumor for highly selective and efficient PDT against cancer.

RESULTS AND DISCUSSION

Characterization of HAOP NPs. The HAOP NPs were fabricated via a double-emulsion method[17] to encapsulate MB and catalase in the aqueous core and BHQ-3 in the PLGA shell, and further modified with c(RGDfK) on the surface. The encapsulation efficiency of MB and catalase in the NP was measured to be 19.5% and 13.1%, respectively. Scanning electron microscopy (SEM) showed that the NPs were well-dispersed with spherical morphology (Figure 1a). The

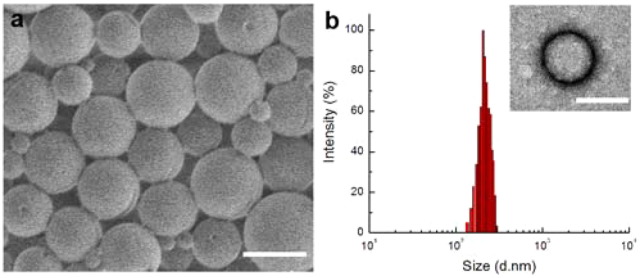

Figure 1. (a) SEM micrographs of HAOP NPs. (b) Size distribution of HAOP NPs characterized by DLS at 25 °C. Inset: TEM micrograph of HAOP NPs. Scale bars: 200 nm.

transmission electron microscopy (TEM) image of HAOP NP clearly revealed its core−shell structure (Figure 1b). The average hydrodynamic diameter of the NPs measured by dynamic light scattering (DLS) was 205 nm (Figure 1b), which did not change for at least 7 days (Figure S1), demonstrating the long-term stability of NPs in culture media. We further compared the size, polydispersity index (PDI), and ζ potential of NPs before and after functionalization with c(RGDfK). Qualitatively, the success of the c(RGDfK) coupling was determined by measuring the ζ potential of the NPs, which was the potential difference between the dispersion medium and the stationary layer of fluid attached to the dispersed particle. The ζ potential of HAOP NPs changed from −24 to −17 mV after conjugation with c(RGDfK) (Table S1), which was caused by the change in surface charge upon modification with the cyclic RGD peptide, confirming the presence of c(RGDfK) at the surface. To investigate the influence of c(RGDfK) on the particle size, PDI and ζ potential, a series of c(RGDfK)-linked NPs were prepared with various c(RGDfK) conjugation ratios, ranging from 1% to 20%. The ζ potential increased 6 mV owing to the additional positive charge from arginine in the peptide (Table S2). Considering the size and dispersibility of the NPs and the yield of peptide coupling to the NPs, c(RGDfK) at a

DOI: 10.1021/ja511420n
J. Am. Chem. Soc. 2015, 137, 1539−1547

mass ratio of 10% to PLGA was used to prepare the HAOP NPs for biological applications.

In Vitro MB Release and Morphological Changes of the HAOP NPs. The H_2O_2-triggered release of MB from HAOP NPs (with/without catalase) was evaluated. After 24 h incubation with 100 μM H_2O_2, about 80% of the MB originally encapsulated within HAOP NPs was released into the medium (Figure 2). Conversely, the release rate of MB from HAOP

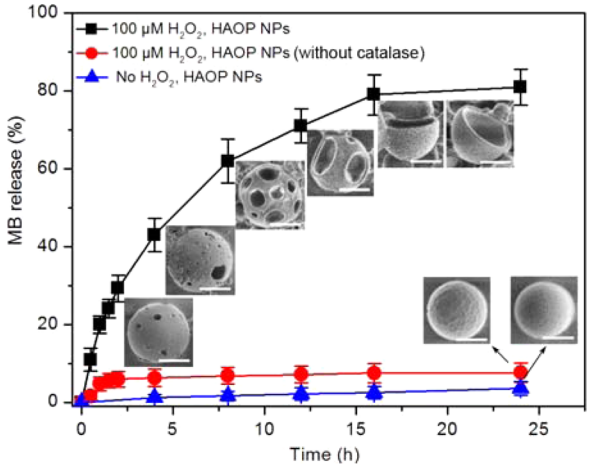

Figure 2. In vitro release profiles of MB from HAOP NPs (with/without catalase) in the presence or absence of 100 μM H_2O_2. Data are means ± SD (n = 3). Insets: SEM micrographs showing the morphological changes of HAOP NPs incubated with 100 μM H_2O_2 for 24 h. Scale bars: 100 nm.

NPs without catalase in the presence of H_2O_2 was much slower, and a very small amount of MB was released within the same period of time. Similarly, HAOP NPs with catalase in the absence of H_2O_2 showed negligible MB release from HAOP NP. These results confirmed that the much higher drug release was specifically triggered by H_2O_2.

The morphological changes of HAOP NPs (with/without catalase) during the course of MB release were also investigated by SEM. The HAOP NPs with catalase in the absence of H_2O_2 or the HAOP NPs without catalase in the presence of H_2O_2 remained intact throughout the entire course of the study (Figure 2). In contrast, the HAOP NPs with catalase were found to rupture the PLGA shell when exposured to H_2O_2. To confirm whether the rupture of NPs was caused by the release of gaseous O_2, an ultrasound imaging was adopted. A large number of O_2 bubbles were observed when HAOP NPs were exposed to a low concentration of H_2O_2 (Figure S2). The formation of gaseous O_2 could be explained by the continuous penetration of H_2O_2 and the subsequent generation of O_2 in the nanoscale core of NPs. The local concentration of O_2 significantly exceeded its solubility, thus the increased internal pressure induced the rupture of HAOP NPs.

After a 2 h incubation with H_2O_2, the pores were clearly observed on the surface of NP, and the pore size became larger and larger. The morphological changes were induced by cavitation, a disruptive force that usually occurs when the liquid is subjected to rapid changes of pressure.[18] As shown by ultrasound imaging, the generation of O_2 bubbles was still observable even at 24 h (Figure S3). As a result of transient formation, gradual growth, and violent collapse of constantly generated O_2 bubbles, a cavitation force was produced to mechanically perforate the shell of NPs and made the holes became larger and larger over time.[15]

Cellular Selectivity. In order to track HAOP NPs in living cancer cells, 3,3′-dioctadecyloxacarbocyanineperchlorate (DiO), a lipophilic dye, was doped into the PLGA shells as a fluorescence tracker. The HAOP NPs at 50 μg mL^{-1} were incubated with $\alpha_v\beta_3$ integrin overexpressed U87-MG cells. After incubation, the fluorescence of U87-MG cells increased gradually along with the incubation time and reached a maximum at 3 h (Figure 3), indicating that the HAOP NPs

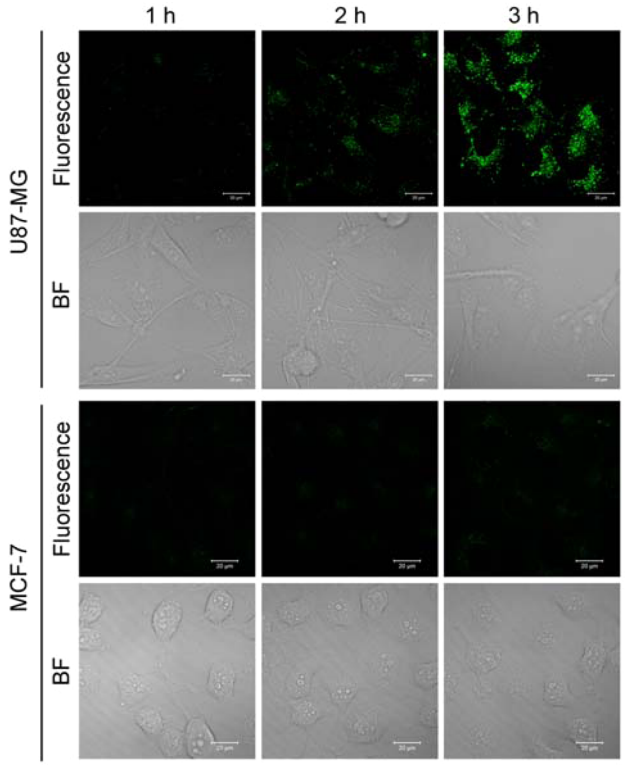

Figure 3. Real-time confocal fluorescence images display the uptake of HAOP NPs by U87-MG and MCF-7 cells. The cells were incubated with HAOP NPs for 1−3 h. Scale bars: 20 μm.

were efficiently uptaken by U87-MG cells. To demonstrate the role of c(RGDfK) moiety in guiding HAOP NPs to $\alpha_v\beta_3$ integrin-rich tumor cells, the HAOP NPs were also incubated with MCF-7 cells that express low levels of $\alpha_v\beta_3$ integrin.[19] Compared to U87-MG cells, only very weak fluorescence was found in MCF-7 cells even incubated for 3 h (Figure 3). The marked difference in fluorescence of these two cell lines suggested the targeting specificity of HAOP NPs toward $\alpha_v\beta_3$ integrin-rich tumor cells.

To further prove that the selective uptake of HAOP NPs was induced by the selective recognition of c(RGDfK) to $\alpha_v\beta_3$ integrin on tumor cells, the cellular uptake of HAOP NPs without c(RGDfK) was studied to compare with HAOP NPs. As shown in Figure 4a, the U87-MG cells displayed strong fluorescence within a 3 h incubation of HAOP NPs, whereas the cells incubated with HAOP NPs without c(RGDfK) showed little fluorescence signal under a similar experimental condition. Furthermore, the internalization of HAOP NPs was blocked when excessive free c(RGDfK) was co-incubated. The results verified that the targeting specificity of HAOP NPs to U87-MG cells was aided by the specific interaction of

DOI: 10.1021/ja511420n
J. Am. Chem. Soc. 2015, 137, 1539−1547

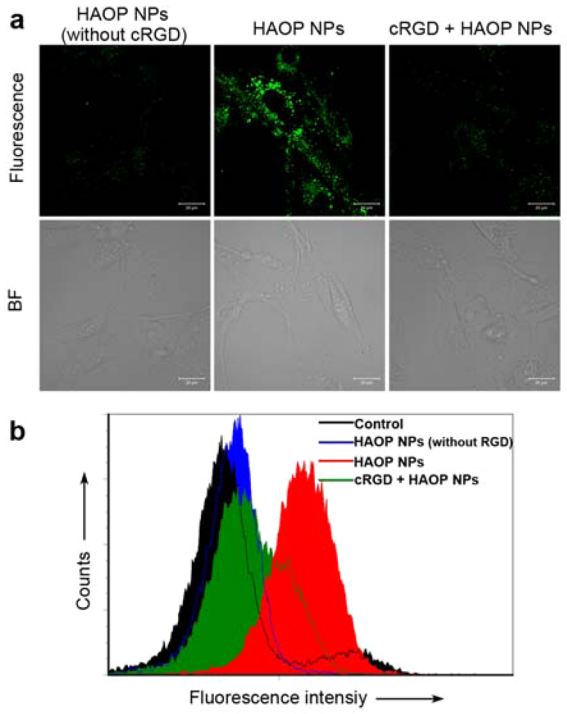

Figure 4. Confocal fluorescence imaging (a) and flow cytometric assay (b) of U87-MG cells incubated with 50 μg mL^{-1} HAOP NPs (without cRGD) or 50 μg mL^{-1} HAOP NPs for 3 h; U87-MG cells pretreated with excessive free cRGD, followed by incubation with 50 μg mL^{-1} HAOP NPs for 3 h. Scale bars: 20 μm.

c(RGDfK) with $\alpha_v\beta_3$ integrin, which was further confirmed by flow cytometry (Figure 4b).

Colocalization Assay. To identify the intracellular location of HAOP NPs, the HAOP NP-loaded U87-MG cells were costained with LysoTracker Red, Mito Tracker Red and Hoechst 33342, respectively. As seen in Figure 5, the fluorescence ascribable to HAOP NPs colocalized well with LysoTracker Red but did not match what was observed in the case of MitoTracker Red and Hoechst 33342. Similar results were observed from the same experiment on SKOV-3 cells (Figure S4 and S5), which also express $\alpha_v\beta_3$ integrin in high levels. Therefore, it is rational to conclude that HAOP NPs entered $\alpha_v\beta_3$ integrin-rich cells via receptor-mediated endocytosis into the lysosome.

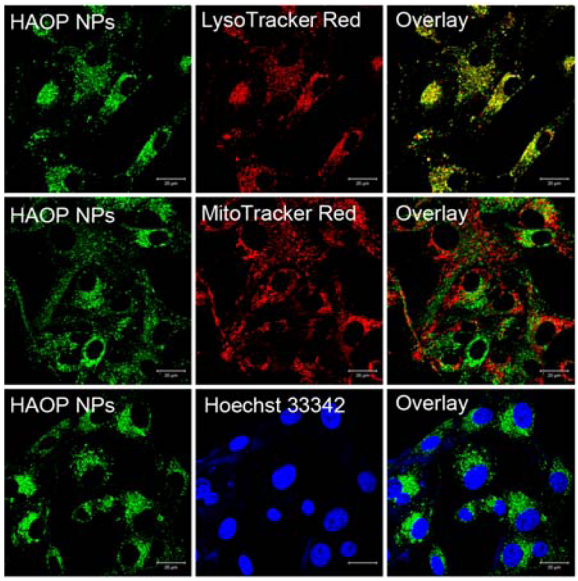

Figure 5. Colocalization images of HAOP NPs in U87-MG cells. Cells were incubated with 50 μg mL^{-1} HAOP NPs for 3 h and then incubated with 100 nM LysoTracker Red, MitoTracker Red, or Hoechst 33342 for 10 min. Scale bars: 20 μm.

H_2O_2 Activatable Generation of $^1O_2$ in Tumor Cells. We first assessed the intracellular H_2O_2 levels with 2′,7′-dichlorofluoresceindiacetate (DCFDA), a H_2O_2 indicator that can be rapidly oxidized by H_2O_2 to emit green fluorescence.[20] Strong fluorescence was observed in U87-MG cells, while the fluorescence was very weak in the cells pretreated with *N*-acetylcysteine (NAC) as an ROS scavenger[21] (Figure S6), confirming the presence of endogenous H_2O_2 in U87-MG cells. Furthermore, a singlet oxygen sensor green (SOSG) reagent was employed to study H_2O_2 activatable generation of $^1O_2$. The fluorescence of SOSG is quenched in its intact form and produces strong fluorescence upon reaction with $^1O_2$.[22] Evaluation of $^1O_2$ production from HAOP NPs in the presence of 100 μM H_2O_2 after 635 nm irradiation was performed by measuring the fluorescence of SOSG at different time points. At the beginning, the fluorescence was very weak (Figure S7), indicating that $^1O_2$ generation was inhibited (OFF) when MB and BHQ-3 were incorporated into HAOP NPs. However, upon addition of H_2O_2, the fluorescence intensity at 525 nm enhanced gradually with incubation time (Figure S7), suggesting that HAOP NPs were activated to produce $^1O_2$ (ON) by H_2O_2. As controls, the release of $^1O_2$ from HAOP NPs in the absence of H_2O_2 and HAOP NPs (without catalase) in the presence of H_2O_2 were also measured. As shown in Figure 6a, negligible increase in fluorescence was observed under these conditions, further validating that the increase of $^1O_2$ was due to H_2O_2 activation.

The $^1O_2$ production within cells was also examined by confocal fluorescence imaging. Figure 6c showed representative confocal images of SOSG fluorescence after 635 nm irradiation in HAOP NP-incubated U87-MG cells. Strong fluorescence of SOSG was observed, which suggested a high level of $^1O_2$ production. In contrast, little or no fluorescence was observed in the cells that pretreated with NAC or incubated with HAOP NPs (without catalase) (Figure 6d, e), demonstrating the specifical H_2O_2 activation to produce $^1O_2$ of HAOP NPs in tumor cells.

Evaluation of PDT Efficacy and Selectivity. Low-dark and high-light cytotoxicity are the necessary properties of a photosensitizer for the application in PDT. The cytotoxicity of HAOP NPs to U87-MG cells was examined in both presence and absence of 635 nm irradiation (100 mW cm^{-2}, 5 min) using MTT assay (Figure S8). In the absence of light, HAOP NPs were basically noncytotoxic, while they exhibited high phototoxicity under irradiation of 30 J cm^{-2}. Furthermore, the phototoxicity increased along with the concentration of HAOP NPs with a half lethal dose (IC_{50}) of 28 μg mL^{-1} at an incubation of 24 h.

To study the PDT effect of HAOP NPs, the cell death induced by HAOP NP-mediated PDT was examined with the dual fluorescence of Annexin V-FITC/propidium iodide (PI), which has been widely used to distinguish viable cells from dead cells of different stages.[23] After U87-MG cells were incubated with 50 μg mL^{-1} NPs for 24 h and then irradiated with a 635 nm laser at a dose of 30 J cm^{-2}, the cells were

DOI: 10.1021/ja511420n
J. Am. Chem. Soc. 2015, 137, 1539−1547

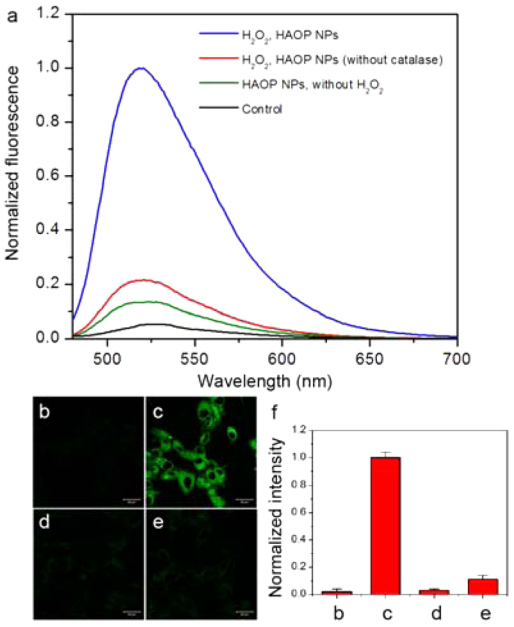

Figure 6. (a) Fluorescence emission spectra of SOSG with different treatments after 635 nm irradiation. Confocal fluorescence images of U87-MG cells with different treatments after 635 nm irradiation: (b) SOSG only; (c) HAOP NPs + SOSG; (d) NAC + HAOP NPs + SOSG; (e) HAOP NPs (without catalase) + SOSG. (f) Normalized average intracellular fluorescence intensity of cells in panels b–e.

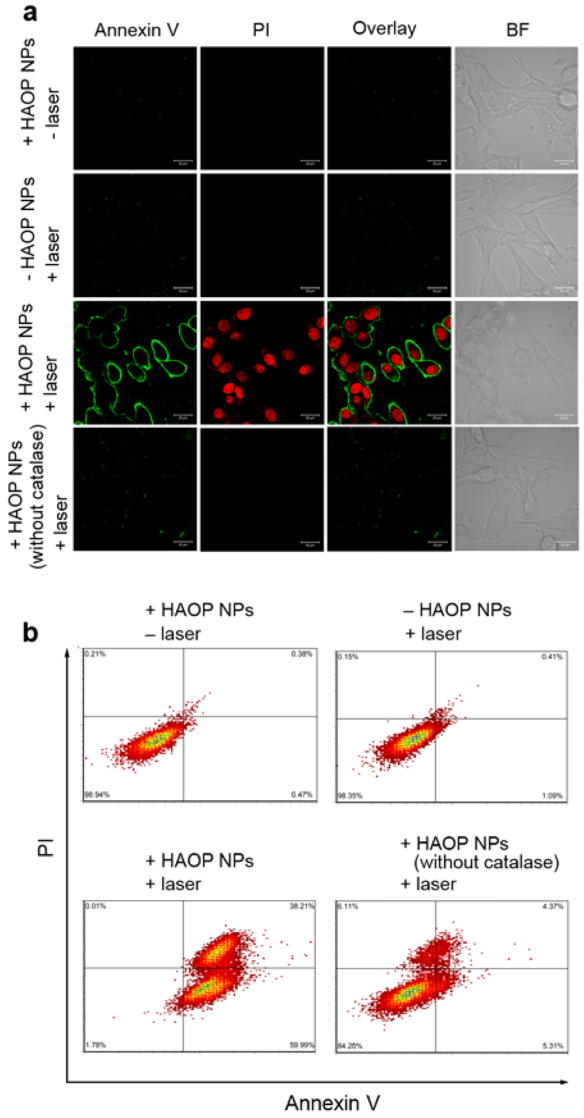

Figure 7. (a) Confocal fluorescence images of Annexin V-FITC/PI stained U87-MG cells and (b) flow cytometric analysis of U87-MG cell death with different treatments. Scale bars: 20 μm.

stained with Annexin V-FITC/PI. As shown in Figure 7a, HAOP NP-treated cells displayed intense fluorescence with apoptotic characteristics after irradiation, indicating apparent cell death. On the other hand, for the cells treated without HAOP NPs or laser, the fluorescence of Annexin V-FITC/PI remained at a background level, which suggested that the cytotoxicity was induced by combination of both HAOP NPs and light. The cells treated with HAOP NPs (without catalase) and irradiation exhibited invisible fluorescence of Annexin V-FITC/PI (Figure 7a), indicating that catalase was essential for H_2O_2 activatable phototoxicity. Similar observations were obtained from flow cytometry assays (Figure 7b). After irradiation, the population of apoptotic cells treated with HAOP NPs was 98.2%, much higher than 15.8% for the cells treated with HAOP NPs (without catalase). These results indicated that HAOP NPs were specifically activated by H_2O_2 to produce high phototoxicity.

To further study the HAOP NP-induced apoptosis in U87-MG cells, acridine orange (AO) was adopted as an indicator for monitoring the integrity of lysosomes.[24] As shown in Figure 8, U87-MG cells in the absence of HAOP NPs under irradiation or in the presence of HAOP NPs without irradiation displayed distinct red fluorescence in lysosomes as well as the untreated cells, indicating the integrity of lysosomes. In contrast, for the cells incubated with 50 μg mL^{-1} HAOP NPs and subsequently irradiated with 635 nm irradiation, the red fluorescence from AO disappeared, and the outer membrane of cells ruptured, indicating the cell death induced by HAOP NP-mediated PDT involved a lysosome-associated pathway.

Normal HaCaT cell line was used as a control model to demonstrate the PDT selectivity of HAOP NPs. After incubation with HAOP NPs for 24 h, the cells were irradiated with 635 nm laser. The cell vitality was determined by MTT assay. The phototoxicity of HAOP NPs on HaCaT cells was much lower than that on U87-MG cells (Figure S9) due to the low expression of $\alpha_v\beta_3$ integrin, demonstrating the high PDT selectivity of HAOP NPs to cancer cells.

Overcoming Tumor Hypoxia by HAOP NPs. Since catalase catalyzes the breakdown of H_2O_2 to generate O_2, we therefore exploited the synergy between catalase and MB to overcome hypoxia in cancer cells and improve the therapeutic efficacy. First, the generation of O_2 from HAOP NPs in U87-MG cells was assessed by a commercially available O_2 probe ($[Ru(dpp)_3]Cl_2$),[25] which showed that the intracellular O_2 levels increased gradually when incubated with HAOP NPs (Figure S10). Furthermore, to investigate the ability of HAOP NPs to overcome hypoxia in vivo, hypoxia-inducible factor (HIF)-1α staining assay[26] was carried out to evaluate hypoxic conditions in the tumor with or without HAOP NPs treatment. As shown in Figure 9, the tumor tissues of the untreated group were stained dark brown and displayed intense immunofluorescence with hypoxic characteristics, indicating the accumulation of HIF-1α under hypoxic conditions. Similarly, the group treated with HAOP NPs (without catalase) also showed a high-

DOI: 10.1021/ja511420n
J. Am. Chem. Soc. 2015, 137, 1539–1547

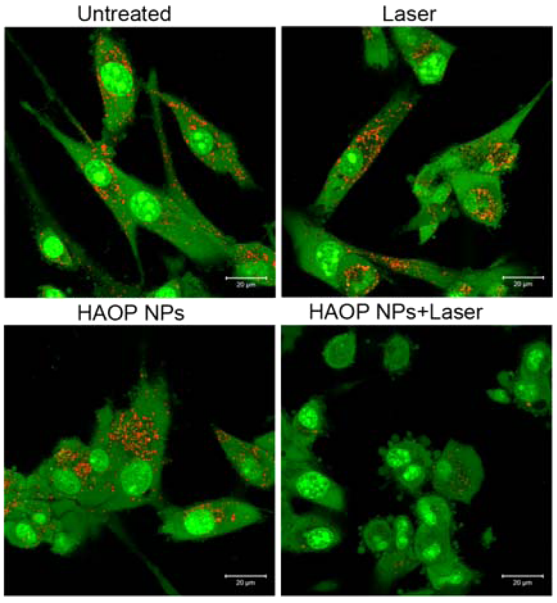

Figure 8. Confocal fluorescence images of AO staining to investigate lysosomal integrity of U87-MG cells with different treatments. AO was excited at 488 nm to emit green fluorescence (515−545 nm) in cytosol and nuclei and red fluorescence (610−640 nm) in lysosomes. Scale bars: 20 μm.

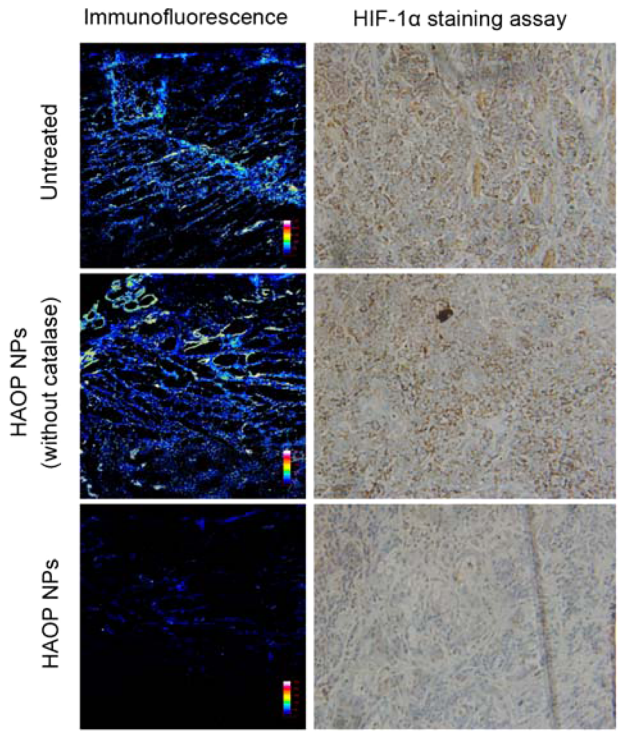

Figure 9. Immunofluorescence staining with HIF-1α antibodies and corresponding HIF-1α staining of tumor slides from U87-MG tumor-bearing mice treated with HAOP NPs or HAOP NPs (without catalase) at a dose of 10 mg kg^{-1}.

level expression of HIF-1α in tumor cells. In contrast, for the group treated with HAOP NPs, the immonufluorescence of tumor tissues was very weak, which suggested that the expression of HIF-1α significantly decreased owing to the generated O_2 in tumor that overcame the hypoxia by catalase-loaded HAOP NPs.

In Vivo PDT on Subcutaneous Tumor-Bearing Mice. The in vivo phototoxicity of HAOP NPs to tumor was investigated in U87-MG tumor-bearing mice. The PDT effects were assessed by monitoring the changes of relative tumor volumes (Figure 10a). After HAOP NP-mediated PDT, tumor

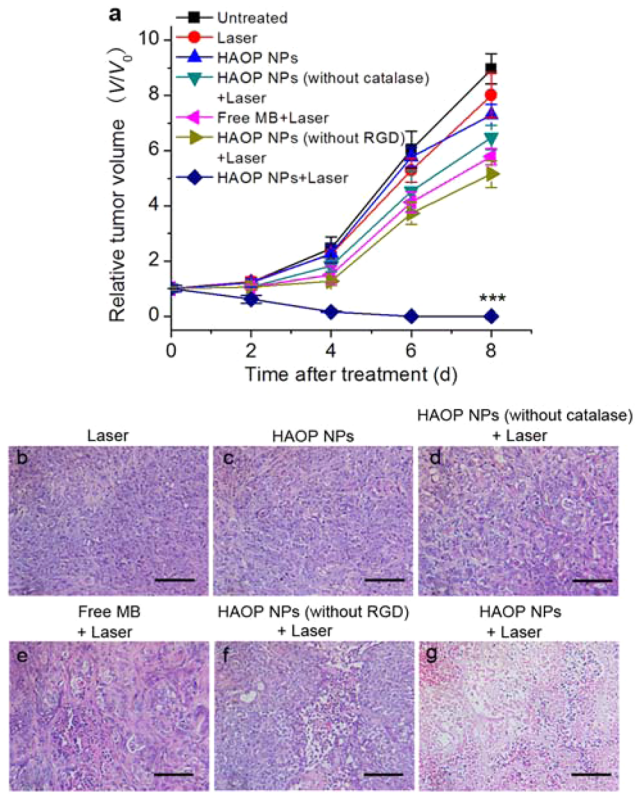

Figure 10. (a) Change of relative tumor volume (V/V_0) upon different treatments. Data are means ± SD (n = 6), ***P < 0.001 compared to other groups using a one-way ANOVA. Tumors at 24 h post-treatment and corresponding H&E staining of tumor slides: (b) 635 nm laser irradiation only; (c) HAOP NPs injection only; (d) HAOP NPs (without catalase) injection and irradiation; (e) free MB injection and irradiation; (f) HAOP NPs (without RGD) injection and irradiation; (g) HAOP NPs injection and irradiation. Necrotic cells show increased eosinophilia (pink staining from the eosin dye) and loss of the basophilia in the cytoplasm (blue staining from the hematoxylin dye). Scale bars: 100 μm.

growth was completely inhibited, and the tumor was eliminated after 7 day treatment, while no significant therapeutic effect was observed for laser or HAOP NPs-only control, revealing that HAOP NPs had little dark toxicity and strong phototoxicity. The free MB-mediated PDT showed low treatment efficiency in a hypoxic tumor which was explained by the hypoxia-induced drug resistance effect and lack of tumor targeting. Similarly, the groups treated with HAOP NPs without catalase or RGD exhibited lower PDT efficiency on inhibiting tumor growth compared with that of HAOP NPs, validating the important roles of catalase and RGD in H_2O_2-activatable PDT in vivo. H&E staining assay was also performed to evaluate the treatment efficacy on the tumors with different treatments. Prominent necrosis was observed in tissue sections from the group treated by HAOP NP-mediated PDT (Figure 10g), while no obvious necrosis was observed in the tumor tissues from other groups (Figures 10b−f and S11). The results confirmed high in vivo PDT efficiency of HAOP NPs owing to

DOI: 10.1021/ja511420n
J. Am. Chem. Soc. 2015, 137, 1539−1547

overcoming the hypoxia-induced drug resistance effect through self-sufficiency of O_2.

Moreover, a survival study was conducted. Survival was significantly prolonged in mice treated with HAOP NP-mediated PDT compared to other groups (Figure 11), further

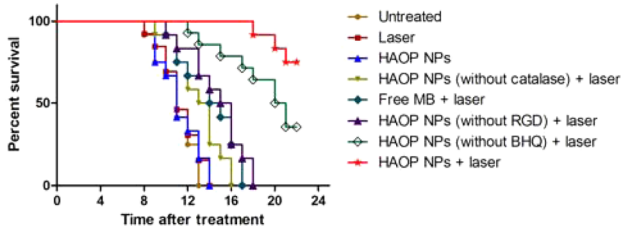

Figure 11. Survival rates of tumor-bearing mice with different treatments indicated (n = 12).

confirming the high PDT efficacy of HAOP NPs. It is noteworthy that the survival rate of HAOP NPs (without BHQ) treated mice was much lower than that of HAOP NPs group, although the PDT activity of HAOP NPs (without BHQ) was similar to that of HAOP NPs at cellular level (Figure S12). The result suggested that BHQ was essential for H_2O_2-activitable function in vivo, which could minimize nonspecific phototoxicity to reduce side effects.

To evaluate the side effects, H&E staining with the organ tissues (e.g., heart, intestine, kidneys, liver, lung, and spleen) of mice after HAOP NP-mediated PDT was performed. Tumors were ablated after 7 day treatment of PDT, while no abnormalities were observed in organ tissues compared with those of the age-matched healthy mice without treatment (Figure S13), confirming the high selectivity to tumor and minimal off-target damage of HAOP NP-mediated PDT.

CONCLUSION

We have successfully developed a new $\alpha_v\beta_3$ integrin-targeted, H_2O_2-activatable, and O_2-evolving NP to achieve selective and highly efficient PDT for cancer treatment. Such a H_2O_2-responsive PDT agent can be used for the spatiotemporally controllable release of $^1O_2$. The controllable PDT activity and the cancer cell-targeting feature led to high PDT selectivity to cancer cells and prevent the damage to normal cells, which greatly lowered the side effects. Moreover, the new O_2-evolving NP achieved unprecedented self-sufficiency of O_2 in PDT process to overcome the hypoxia-induced drug resistance. The NPs exhibit high selectivity and efficiency for in vivo PDT without adverse effects to normal tissues. Overall, this work provides new insight into the design of smart PDT systems to achieve more precise and effective PDT in O_2-deprived tumor tissue.

EXPERIMENTAL SECTION

Materials and Reagents. Poly(D,L-lactic-*co*-glycolic acid) (PLGA, with a lactide/glycolide molar ratio of 75:25 and an inherent viscosity of 0.17 dL g^{-1}) was obtained from Daigang BIO Engineer Ltd. Co. (Shandong, China). Methylene Blue (MB), catalase, H_2O_2, 1-ethyl-3-[3-(dimethylamino)propyl] carbodiimidehydrochloride (EDC), *N*-hydroxysuccinimide (NHS), 3-(4,5-dimethylthiazol-2-yl)-2,5-diphenyl-tetrazolium bromide (MTT), 9,10-phenan-threnequinone, poly(vinyl alcohol) (PVA, M_W = 57−66 kDa), and 3,3′-dioctadecyloxacarbocya-nineperchlorate (DiO) were all obtained from Sigma-Aldrich (St. Louis, MO, USA). BHQ-3 and DCFDA were purchased from Biosearch Technologies, Inc. c(RGDfK) was obtained from Sangon Biotech Ltd. Co (Shanghai, China). Ultrapure water was prepared using a Millipore Simplicity System (Millipore, Bedford, USA). Annexin V-FITC/PI Cell Apoptosis Kit was obtained from KeyGen Biotech. Co. Ltd. (Nanjing, China).

Fabrication and Characterization of HAOP NPs. HAOP NPs were prepared using a water-in-oil-in-water (W/O/W) double emulsion, solvent diffusion evaporation approach method.[17] A 2.5 mg catalase powder and 2 mg MB were added to 1 mL PVA aqueous solution (10 mg mL^{-1}) and then mixed thoroughly for 15 min. Subsequently, the mixture was emulsified with 2 mL of PLGA solution (5 mg mL^{-1} in CH_2Cl_2) containing BHQ-3 (10 mg mL^{-1}) to obtain the primary W/O emulsion. The primary emulsification was carried out by using an ultrasonicator for 1 min in an ice bath. The primary emulsion was then added to 6 mL of PVA aqueous (20 mg mL^{-1}) and emulsified by using an ultrasonicator for 1 min in an ice bath to form the W/O/W double emulsion. To evaporate CH_2Cl_2 and solidify the NPs, the resultant double emulsion was transferred into 20 mL of ultrapure water and stirred overnight at room temperature. After washing three times with ultrapure water, the PLGA NPs were collected by centrifugation. The reaction process for conjugation of NH_2-containing c(RGDfK) with carboxyl-containing PLGA NPs via covalent amide bond involves EDC/NHS activation of carboxylic acids and the following amidation reaction.[27] The NPs suspension (150 μL, 10 mg mL^{-1}) was treated with 400 mM EDC and 100 mM NHS in water for 15 min at room temperature with agitation to give the corresponding PLGA-NHS ester. The activated NPs were washed twice using the Amicon Ultra centrifugal filter units to remove unreacted EDC and NHS. And then c(RGDfK) was added into the PLGA NPs suspension at a mass ratio of 10% to PLGA, agitating for 2 h at room temperature. The resulting NPs were washed three times with Amicon Ultra centrifugal filter units and resuspended in water for storage. The peptide content of HAOP NPs was determined by measuring arginine using a fluorimetric assay.[28] The reagent 9,10-phenan-threnequinone was mixed with the sample at a high pH followed by acidification to convert arginine residues to a strongly fluorescent small molecule (λ_{ex}= 312, λ_{em}= 340−570 nm). The surface morphology and size of the as-prepared HAOP NPs were investigated by SEM (Hitachi s-4800 high resolution SEM) on the conductive adhesive tapes. TEM (JEM-2100) measurement was prepared by dropping the solution onto a carbon-coated copper grid following negative staining with 2.0% (w/v) phosphotungstic acid. The particle size and size distribution of HAOP NPs were measured by DLS (a Mastersizer 2000 particle size analyzer) with a fixed scattering angle of 90°. Zeta potential measurements were performed at 25 °C on a Malvern Zeta sizer-Nano Z instrument. An ultrasound imaging system (Toshiba Nemio 30, Japan) was utilized to visualize the O_2 bubbles generated by HAOP NPs in a test tube containing H_2O_2.

In Vitro Release of Payload from the HAOP NPs. The profiles for the in vitro release of payload from NPs were established by dialysis of the HAOP NPs suspensions in PBS. Briefly, 3 mL NPs suspensions (50 μg mL^{-1}) were dialyzed against 15 mL PBS buffer (molecular weight cutoff: 12,000) and gently shaken in a thermostatic rotary shaker at 100 rpm and 37 °C. Samples were removed at different intervals, and an equal amount of the same medium was added to maintain a constant volume. The MB concentration corresponding to 100% release is 2.2 mg L^{-1}.

Cell Culture and Confocal Fluorescence Imaging. Human glioblastoma-astrocytoma cell line (U87-MG cells), human breast cancer cell line (MCF-7 cells), human caucasian ovary adenocarcino-ma cell line (SKOV-3 cells), and human epidermal cell line (HaCaT cells) were maintained following protocols provided by the American type Tissue Culture Collection. Cells were seeded at a density of 1 × 10^6 cells mL^{-1} in RPMI 1640 supplemented with 10% FBS, $NaHCO_3$ (2 g L^{-1}), and 1% antibiotics (penicillin/streptomycin, 100 U mL^{-1}). The cells were maintained in a humidified incubator at 37 °C, in 5% CO_2/95% air. One day before imaging, cells were passed and plated on 18 mm glass bottom dishes. Cell imaging was carried out after washing cells with PBS for three times. Confocal fluorescence imaging studies were performed with a ZEISS Laser Scanning Microscope (Zeiss LSM 710).

DOI: 10.1021/ja511420n
J. Am. Chem. Soc. 2015, 137, 1539−1547

In Vitro Cytotoxicity Assay. MTT assay was carried out to investigate the dark toxicity and phototoxicity of HAOP NPs. U87-MG cells were first seeded to two 96-well plates at a seeding density of 1×10^4 cells per well in 200 μL complete medium, which was incubated at 37 °C for 24 h. After rinsing with PBS, U87-MG cells were incubated with 200 μL culture media containing serial concentrations of HAOP NPs for 24 h. One plate was kept in the dark for studying dark toxicity, and another plate was irradiated using a 635 nm laser (Changchun Laser Optoelectronics Technology Co., Ltd., China) at a power of 100 mW cm^{-2} for 5 min. Afterward, the cells were grown for another 24 h. Then, 20 μL of 5 mg mL^{-1} MTT solution in pH 7.4 PBS was added to each well. After a 4 h incubation, the medium containing unreacted MTT was removed carefully, and 150 μL of DMSO was added to each well to dissolve the formazan crystals. After 1 h the absorbance (abs.) was measured at 490 nm in a TRITURUS microplate reader. The cell viability was then determined by the following equation: cell viability (%) = (mean of abs. value of treatment group/mean abs. value of control) × 100%. Calculation of the half lethal dose (IC_{50}) values was done according to Huber and Koella.[29]

Flow Cytometry Analysis. To study the cell apoptosis induced by HAOP NPs and HAOP NPs (without catalase) after irradiation on U87-MG cells, a flow cytometric assay of Annexin V-FITC and PI costaining was employed. Cells were harvested, rinsed in PBS, resuspended, and determined by flow cytometry using Cytomics FC500 Flow Cytometry (Beckman Coulter Ltd.). All experiments detected at least 10,000 cells, and the data were analyzed with FCS Express V3.

Study on Intracellular Generation of O_2 from HAOP NPs. The intracellular generation of O_2 was investigated by confocal fluorescence imaging with $[(Ru(dpp)_3)]Cl_2$, an O_2 sensing probe that the fluorescence can be strongly quenched by O_2. U87-MG cells were incubated with 5 μM $[Ru(dpp)_3]Cl_2$ for 4 h and further incubated with 50 μg mL^{-1} HAOP NPs (containing catalase only) for 24 h. The cells were excited at 488 nm, and the emission was collected between 600 and 700 nm.

Animal and Tumor Model. Specific pathogen-free (SPF) female BALB/c mice, 5−6 weeks of age, were purchased from Shanghai Laboratory Animal Center and bred in an axenic environment. All animal operations were in accord with institutional animal use and care regulations approved by the Model Animal Research Center of Nanjing University (MARC). U87-MG tumor model was established by subcutaneous injection of U87-MG cells (1×10^6) into the selected positions of the nude mice. During treatment, mice were anesthetized with 2.5% isoflurane in oxygen delivered at a flow rate of 1.5 L min^{-1}. Tumors were then allowed to grow to 5−8 mm in diameter. To determine tumor volume, the greatest longitudinal diameter (length) and the greatest transverse diameter (width) from each tumor were determined using a vernier caliper. Each tumor's volume, based on the caliper measurements, was calculated using the following formula: tumor volume = length × width^2 × 0.5.

In Vivo PDT on Subcutaneous Tumor Model. In vivo PDT was performed using U87-MG tumor-bearing mice. The mice were randomly divided into seven groups and subjected to the following treatments: group 1, untreated; group 2, laser only; group 3, intravenous injection of HAOP NPs only; group 4, intravenous injection of HAOP NPs (without catalase) combined with irradiation; group 5, intravenous injection of free MB combined with irradiation; group 6, intravenous injection of HAOP NPs (without RGD) combined with irradiation; and group 7, intravenous injection of HAOP NPs combined with irradiation. HAOP NPs (without catalase) of 10 mg kg^{-1}, free MB of 0.4 mg kg^{-1}, HAOP NPs (without RGD), or HAOP NPs of 10 mg kg^{-1} in PBS were intravenously injected into groups 4−7. After 24 h, PDT treatment was performed on groups 4−7 by irradiating the tumor region with a 635 nm laser at a power of 100 mW cm^{-2} for 5 min. The therapeutic effects were evaluated by survival assay and monitoring the changes of relative tumor volumes.

HIF-1α Staining. U87-MG tumor-bearing mice were randomly divided into three groups and subjected to the following treatments: group 1, untreated; group 2, intravenous injection of HAOP NPs; and group 3, intravenous injection of HAOP NPs (without catalase). The dose of HAOP NPs or HAOP NPs (without catalase) injected was 10 mg kg^{-1}. After 24 h treatment, the mice were sacrificed, and the tumors were harvested and fixed in 10% formaldehyde for HIF-1α staining.

H&E Staining. H&E staining was performed according to aprotocol provided by the vendor (BBC Biochemical). Briefly, 8 μm cryogenic slides were prepared and fixed with 10% formalin for about 30 min at room temperature. After washing with running water for 5 min, the slides were treated with gradient concentrations of alcohol (100, 95, and 70%), each for 20 s. The hematoxylin staining was performed for about 3 min and washed with water for 1 min. The eosin staining was performed for about 1 min. The slides were washed, treated with xylene, and mounted with Canada balsam. The images were acquired on a Nikon Eclipse 90i microscope.

■ ASSOCIATED CONTENT

Ⓢ Supporting Information

Supplementary tables and figures. This material is available free of charge via the Internet at http://pubs.acs.org.

■ AUTHOR INFORMATION

Corresponding Authors

*heweij69@nju.edu.cn

*zguo@nju.edu.cn

Author Contributions

†These authors contributed equally.

Notes

The authors declare no competing financial interest.

■ ACKNOWLEDGMENTS

We thank the National Basic Research Program of China (2015CB856300 and 2011CB935800) and National Natural Science Foundation of China (nos. 21271100, 91213305, 91413116, 10979019, 21131003, and 21361140352) for financial support.

■ REFERENCES

(1) Gross, S.; Gilead, A.; Scherz, A.; Neeman, M.; Salomon, Y. *Nat. Med.* **2003**, *9*, 1327−1331.

(2) Lovell, J. F.; Liu, T. W. B.; Chen, J.; Zheng, G. *Chem. Rev.* **2010**, *110*, 2839−2857.

(3) (a) Chen, H.; Xiao, L.; Anraku, Y.; Mi, P.; Liu, X.; Cabral, H.; Inoue, A.; Nomoto, T.; Kishimura, A.; Nishiyama, N.; Kataoka, K. *J. Am. Chem. Soc.* **2014**, *136*, 157−163. (b) Cheng, Y.; Meyers, J. D.; Broome, A. M.; Kenney, M. E.; Basilion, J. P.; Burda, C. *J. Am. Chem. Soc.* **2011**, *133*, 2583−2591. (c) Zhen, Z.; Tang, W.; Chuang, Y. J.; Todd, T.; Zhang, W.; Lin, X.; Niu, G.; Liu, G.; Wang, L.; Pan, Z.; Chen, X.; Xie, J. *ACS Nano* **2014**, *8*, 6004−6013.

(4) Henderson, B. W.; Fingar, V. H. *Cancer Res.* **1987**, *47*, 3110−3114.

(5) Thomas, S.; Harding, M. A.; Smith, S. C.; Overdevest, J. B.; Nitz, M. D.; Frierson, H. F.; Tomlins, S. A.; Kristiansen, G.; Theodorescu, D. *Cancer Res.* **2012**, *72*, 5600−5612.

(6) Vaupel, P.; Thews, O.; Hoeckel, M. *Med. Oncol.* **2001**, *18*, 243−259.

(7) Brown, J. M.; Wilson, W. R. *Nat. Rev. Cancer* **2004**, *4*, 437−447.

(8) Mitchell, J. B.; McPherson, S.; DeGraff, W.; Gamson, J.; Zabell, A.; Russo, A. *Cancer Res.* **1985**, *45*, 2008−2011.

(9) Yue, X.; Yanez, C. O.; Yao, S.; Belfield, K. D. *J. Am. Chem. Soc.* **2013**, *135*, 2112−2115.

(10) Ethirajan, M.; Chen, Y.; Joshi, P.; Pandey, R. K. *Chem. Soc. Rev.* **2011**, *40*, 340−362.

(11) Yogo, T.; Urano, Y.; Mizushima, A.; Sunahara, H.; Inoue, T.; Hirose, K.; Iino, M.; Kikuchi, K.; Nagano, T. *Proc. Natl. Acad. Sci. U.S.A.* **2008**, *105*, 28−32.

DOI: 10.1021/ja511420n
J. Am. Chem. Soc. 2015, 137, 1539−1547

(12) (a) Tian, J.; Ding, L.; Xu, H. J.; Shen, Z.; Ju, H.; Jia, L.; Bao, L.; Yu, J. S. *J. Am. Chem. Soc.* **2013**, *135*, 18850−18858. (b) He, H.; Lo, P. C.; Ng, D. K. P. *Chem.—Eur. J.* **2014**, *20*, 6241−6245. (c) Koide, Y.; Urano, Y.; Yatsushige, A.; Hanaoka, K.; Terai, T.; Nagano, T. *J. Am. Chem. Soc.* **2009**, *131*, 6058−6059. (d) Zhu, Z.; Tang, Z.; Phillips, J. A.; Yang, R.; Wang, H.; Tan, W. *J. Am. Chem. Soc.* **2008**, *130*, 10856−10857.
(13) Trachootham, D.; Alexandre, J.; Huang, P. *Nat. Rev. Drug Discovery* **2009**, *8*, 579−591.
(14) (a) Chen, H.; He, W.; Guo, Z. *Chem. Commun.* **2014**, *50*, 9714−9717. (b) de Gracia Lux, C.; Joshi-Barr, S.; Nguyen, T.; Mahmoud, E.; Schopf, E.; Fomina, N.; Almutairi, A. *J. Am. Chem. Soc.* **2012**, *134*, 15758−15764. (c) Broaders, K. E.; Grandhe, S.; Fréchet, J. M. *J. Am. Chem. Soc.* **2011**, *133*, 756−758.
(15) Ke, C. J.; Chiang, W. L.; Liao, Z. X.; Chen, H. L.; Lai, P. S.; Sun, J. S.; Sung, H. W. *Biomaterials* **2013**, *34*, 1−10.
(16) He, X.; Wu, X.; Wang, K.; Shi, B.; Hai, L. *Biomaterials* **2009**, *30*, 5601−5609.
(17) Tu, F.; Lee, D. *Langmuir* **2012**, *28*, 9944−9952.
(18) Chung, M. F.; Chen, K. J.; Liang, H. F.; Liao, Z. X.; Chia, W. T.; Xia, Y.; Sung, H. W. *Angew. Chem., Int. Ed.* **2012**, *51*, 10089−10093.
(19) Yuan, Y.; Kwok, R. T.; Tang, B. Z.; Liu, B. *J. Am. Chem. Soc.* **2014**, *136*, 2546−2554.
(20) Shim, M. S.; Xia, Y. *Angew. Chem., Int. Ed.* **2013**, *125*, 7064−7067.
(21) Liu, L.; Zhang, Z.; Xing, D. *Free Radic. Biol. Med.* **2011**, *51*, 53−68.
(22) Master, A. M.; Livingston, M.; Oleinick, N. L.; Sen Gupta, A. *Mol. Pharmaceutics* **2012**, *9*, 2331−2338.
(23) Thomas, A. P.; Saneesh Babu, P. S.; Asha Nair, S.; Ramakrishnan, S.; Ramaiah, D.; Chandrashekar, T. K.; Srinivasan, A.; Radhakrishna Pillai, M. *J. Med. Chem.* **2012**, *55*, 5110−5120.
(24) Chen, H.; Xiao, L.; Anraku, Y.; Mi, P.; Liu, X.; Cabral, H.; Inoue, A.; Nomoto, T.; Kishimura, A.; Nishiyama, N.; Kataoka, K. *J. Am. Chem. Soc.* **2014**, *136*, 157−163.
(25) Gryczynski, I.; Gryczynski, Z.; Rao, G.; Lakowicz, J. R. *Analyst* **1999**, *124*, 1041−1044.
(26) Jin, C. S.; Lovell, J. F.; Chen, J.; Zheng, G. *ACS Nano* **2013**, *7*, 2541−2550.
(27) Wang, C.; Yan, Q.; Liu, H. B.; Zhou, X. H.; Xiao, S. J. *Langmuir* **2011**, *27*, 12058−12068.
(28) Graf, N.; Bielenberg, D. R.; Kolishetti, N.; Muus, C.; Banyard, J.; Farokhzad, O. C.; Lippard, S. J. *ACS Nano* **2012**, *6*, 4530−4539.
(29) Huber, W.; Koella, J. C. *Acta Trop.* **1993**, *55*, 257−261.

DOI: 10.1021/ja511420n
J. Am. Chem. Soc. 2015, 137, 1539−1547